

## Article

# Redoxless Electrochemical Capacitance Spectroscopy for Investigating Surfactant Adsorption on Screen-Printed Carbon Electrodes

Tzong-Jih Cheng , Hsien-Yi Hsiao, Pei-Chia Tsai  and Richie L. C. Chen

Department of Biomechanics Engineering, College of Bio-Resources and Agriculture, National Taiwan University, Taipei 10617, Taiwan; f92631001@ntu.edu.tw (H.-Y.H.); r10631004@ntu.edu.tw (P.-C.T.); rlcchen@ntu.edu.tw (R.L.C.C.)

\* Correspondence: tzongjih@ntu.edu.tw

**Abstract:** Electrochemical impedance spectroscopy (EIS) is a sensitive analytical method for surface and bulk properties. Classical EIS and derived electrochemical capacitance spectroscopy (ECS) with a redox couple are label-free approaches for biosensor development, but doubts arise regarding interpretability when a redox couple is employed (redox EIS) due to interactions between electroactive probes and interfacial charges or forced potential. Here, we demonstrated redoxless ECS for directly determining surfactant adsorption on screen-printed carbon electrodes (SPCEs), validated through a simulation of equivalent circuits and the electrochemistry of electronic dummy cells. Redoxless ECS provides excellent capacitance plot loci for quantifying the interfacial permittivity of dielectric layers on electrode surfaces. Redoxless ECS was compared with redox EIS/ECS, revealing a favorable discrimination of interfacial capacitances under both low and high SDS coverage on SPCEs and demonstrating potential for probeless (reagentless) sensing. Furthermore, the proposed method was applied in an electrolyte without a redox couple and bare electrodes, obtaining a high performance for the adsorption of surfactants Tween-20, Triton-X100, sodium dodecyl sulfate, and tetrapropylammonium bromide. This approach offers a simple and straightforward means for a semi-quantitative evaluation of small molecule interactions with electrode surfaces. Our proposed approach may serve as a starting point for future probeless (reagentless) and label-free biosensors based on electrochemistry, eliminating disturbance with surface charge properties and minimizing forced potential bias by avoiding redox couples. An unambiguous and quantitative determination of physicochemical properties of biochemically recognizable layers will be relevant for biosensor development.

**Keywords:** electrochemical capacitance spectroscopy; surfactant; redoxless; biosensor; screen-printed carbon electrode



**Citation:** Cheng, T.-J.; Hsiao, H.-Y.; Tsai, P.-C.; Chen, R.L.C. Redoxless Electrochemical Capacitance Spectroscopy for Investigating Surfactant Adsorption on Screen-Printed Carbon Electrodes. *Chemosensors* **2023**, *11*, 343. <https://doi.org/10.3390/chemosensors11060343>

Academic Editor: Núria Serrano

Received: 24 April 2023

Revised: 2 June 2023

Accepted: 9 June 2023

Published: 11 June 2023



**Copyright:** © 2023 by the authors. Licensee MDPI, Basel, Switzerland. This article is an open access article distributed under the terms and conditions of the Creative Commons Attribution (CC BY) license (<https://creativecommons.org/licenses/by/4.0/>).

## 1. Introduction

Electrochemical impedance spectroscopy (EIS), an analytical method described in detail in many papers and textbooks [1,2], is sensitive to both surface phenomena and bulk properties [3–5]. Therefore, EIS is considered as extremely useful in numerous electrochemical applications, such as corrosion studies [6,7], the monitoring of fuel cells [8], and bioanalytical applications [9]. EIS is considered as label-free because the presence of the target analyte can be detected directly without the requirement of any labeling or amplification procedure [10,11]. This advantage means that EIS can be implemented in bio-sensor-based point-of-care products, which are currently receiving considerable scientific interest [12]. In the direct label-free approach of EIS, it is generally expected that, when a modified electrode with a suitable biochemical recognition element is exposed to a solution containing its complementary analyte, the affinity complex that forms will resist the penetration of the electrode surface by redox probes from the solution. Therefore, the obstruction directly leads to an increase in electrochemical impedance, which

is often observed as an increase in the charge transfer resistance ( $R_{ct}$ ). In the majority of studies, the increase in  $R_{ct}$  has been used as an output signal corresponding to the amount of captured analyte. Most researchers have attempted to reduce the detection limit by modifying the interface, and the correspondence between the impedance spectrum and physicochemical behavior of the electrode interface is often neglected. The viewpoint that the capture of complex biomolecules from a non-constant electric double layer rarely yields EIS results that are controlled only by the analyte concentration has recently been raised by investigators [13].

The electric double layer, ionic strength of the contacting solution, electron transfer across the electrode/electrolyte interface, electrolyte's resistivity, and electrode's material properties, among other factors, determine the EIS signals. Consequently, the measured EISs are usually fitted to an a-priori-based electric model of the system to obtain useful information. In EIS-based biosensors, redox-couple probes, incorporated into the electrolyte, detect changes in  $R_{ct}$  dominated by the redox probes that occur at the electrode/electrolyte interface. As the recognition element binds to the electrode's surface, the redox couple's interaction with the electrode is affected, altering  $R_{ct}$  and the impedance. The impedance signal's main parameter is reported to be the charge of modified biochemical molecules on the electrode surface [13–15]. The DC potential bias applied to the electrodes to perform EIS measurements affects the electrical properties of the electrode–electrolyte interface and modified biochemical molecules on the electrode's surface.

In conventional EIS, a high-ionic-strength electrolyte is used to assume a constant electric double-layer capacitance at the conductive electrode interface. However, if electrodes are modified with biochemical molecules, the equivalent capacitance of the interface may not solely be the electric double-layer capacitance, but rather a composite capacitance. To address this issue, researchers have proposed electrochemical capacitance spectroscopy (ECS) to assess the physicochemical characteristics of the electrode interface [16,17].

The ECS approach has been shown to be superior to the Nyquist impedance plot of EIS for obtaining the capacitance of an electrode [18] and DNA sensing [19]. Researchers have proposed a redox-tethered ECS method to avoid the need to add a redox couple to the electrolyte [20–22]. Redox-tethered ECS has been used to biosense biomarkers such as dengue nonstructural protein 1 [20], C-reactive protein [23], human prostatic acid phosphatase [24], and interleukin-6 [21]. Two comparative studies have indicated that the impedimetry with a redox couple and redox-tethered capacitive approaches exhibit a similar analytical performance [25,26]. A well-known research team has proposed useful guidance for decisions that should be made during the development of electrochemical biosensors based on the resistive (EIS) or capacitive (ECS) approach [27]. The redox-tethered ECS method may resolve the issue of the redox couple becoming concentrated near the electrode interface due to the charge of biomolecules on the electrode surface, and the method is based on capacitance measurement, avoiding the aforementioned reliance on using  $R_{ct}$  as a quantitative parameter.

ECS can determine the interfacial capacitance, including the electric double-layer and modified-layer capacitance, without using  $R_{ct}$  as a quantitative parameter. Redoxless EIS and ECS tests do not require a redox couple and are conducted through non-Faradaic processes where electron transfer effects are not dominant. Though redoxless EIS has been common in corrosion research, it has received less attention from biosensor researchers. A few researchers have attempted to apply redoxless EIS or ECS to the investigation of the dielectric properties of self-assembled monolayers (SAMs) [28], biomimetic deposition of calcium phosphate [29], and direct detection of lead ions in tap water [30]. Recently, redoxless impedimetric methods have been applied to biochemical analysis, including the detection of ions [31], D-dimers [32], and low-molecular-weight triamterene [33]. Phase-monitoring EIS was used to demonstrate a reagentless insulin-biosensor-modified antibody, and phase-change analyses were sensitive at low frequencies (0.1–1 Hz) [34]. These reports have inspired the development of reagentless and redoxless capacitive biosensors.

Surfactant adsorption serves as a model used to evaluate interfacial surfaces in biosensors. Cationic surfactant adsorption at the solid–aqueous interface can be reviewed for the background [35]. Various electrochemistry methods, such as galvanostatic cycling, cyclic voltammetry, and EIS, investigate the effect of surfactants on the carbon electrode capacitance [36]. Polycrystalline Ni electrode adsorption was assessed using differential capacitance at a constant 80 Hz frequency [37]. The sensitivity and resolution of QCMs and ellipsometers were evaluated using the model of adsorption for small-molecule surfactants [38]. A well-defined affinity mechanism provides a straightforward approach and procedure to verify if an interface characteristic can be determined. The use of low-molecular-weight surfactants is crucial for preliminary assessments of the analytical performance of candidate approaches as it challenges the detection limit of analytical methods.

The goal of this study was to develop a redoxless ECS approach for characterizing interfacial capacitance in EIS-based biosensors, aiming to overcome the ambiguity caused by changes in  $R_{ct}$  as a quantitative parameter due to redox couples. The objective was to establish the approach as an analytical platform for capacitive biosensor development. The study involved simulating electronic equivalent circuits to establish the theoretical basis for translating EIS to ECS. To validate the consistency and validity of the proposed ECS approach with the theory, experiments were conducted using an electrochemical analyzer with dummy samples. The adsorption of surfactants on an SPCE was utilized as a model to confirm the quantitative analysis of capacitive changes in low-molecular-weight molecules adsorbed at an electrode interface. By eliminating the need for redox-couple-containing electrolytes, this approach simplifies the preparation and storage process of biosensors.

## 2. Materials and Methods

### 2.1. Electronic Dummy Cells for Electrochemistry

Resistors (0.1 k $\Omega$ –10 M $\Omega$ , tolerance:  $\pm 1\%$ ) and ceramic capacitors (1 nF–10  $\mu$ F, tolerance =  $\pm 10\%$ ) were used to develop various equivalent circuits for electrochemical dummy cells, as illustrated in Figure 1a. Five combinations of a resistor in parallel with a capacitor were arranged in a dummy cell. One dummy cell comprised a resistor ( $R_{ct} = 1$  M $\Omega$ ) in parallel with a capacitor with one of five capacitances ( $C_{dl} = 10$   $\mu$ F, 1  $\mu$ F, 0.1  $\mu$ F, 0.01  $\mu$ F, or 1 nF), and the other comprised a capacitor ( $C_{dl} = 1$   $\mu$ F) with a resistor with one of five resistances ( $R_{ct} = 10$  M $\Omega$ , 1 M $\Omega$ , 0.1 M $\Omega$ , 0.1 M $\Omega$ , or 1 k $\Omega$ ). Both of these dummy cells contained the same series resistance of  $R_s = 100$   $\Omega$ . The dummy cells were used with a commercial electrochemical analyzer for the EIS experiments.

### 2.2. Reactants and Electrochemical Measurements

Sodium dodecyl sulfate (SDS) was purchased from Showa Kako Corp. (Osaka, Japan), Tetrapropylammonium bromide (TPAB) was purchased from Acros Organics (Morris Plains, NJ, USA), and Triton X-100 and Tween-20 were purchased from Sigma-Aldrich (St. Louis, MO, USA). To prepare 0.1 M phosphate buffer (pH 7.0) solution, 0.1 M NaH<sub>2</sub>PO<sub>4</sub> and 0.1 M Na<sub>2</sub>HPO<sub>4</sub> were mixed and then regulated to the required pH using a NaOH solution. Additionally, 10 mM ferrocyanide or ferrocyanoide was prepared in 0.1 M phosphate buffer (pH 7.0) or 0.1 M HCl solution.

Electrochemical measurements were conducted using an Autolab PGSTAT 12 instrument (EchoChemie, Utrecht, The Netherlands) equipped with an FRA2 module controlled by NOVA v.1.1 software; the latter was used for impedance measurements. All electrochemical data were obtained at room temperature (298 K). The electrochemical potentials in this paper are stated with respect to Ag|AgCl reference electrodes (3 M KCl, RE-1S, Great & Best Co., Ltd., Taipei, Taiwan). An SPCE with an area of 0.45 mm<sup>2</sup> and a platinum coil were used as the working and counter electrodes, respectively.

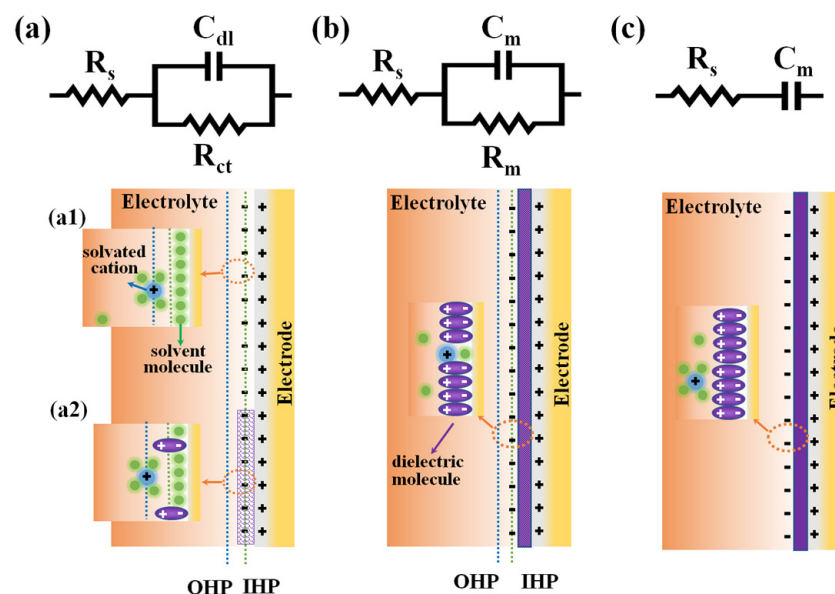


**Figure 1.** Schematic representation and typical equivalent circuits for electrode/electrolyte interfaces: (a) without coating (a1) or with slight coating (a2) (Randles-type); (b) with an imperfect coating (Randles-type); (c) with a perfect coating (Helmholtz-type).  $R_s$ , solution resistance;  $C_{dl}$ , electric double-layer capacitance;  $R_{ct}$ , charge transfer resistance;  $C_m$ , dielectric layer capacitance;  $R_m$ , dielectric layer resistance. IHP and OHP refer to the inner and outer Randles planes, respectively.

All EIS measurements were conducted using a typical three-electrode cell setup and at a hold potential (bias) of 0.0 or 0.3 V for redoxless and redox processes, respectively; an aqueous solution of 0.1 M phosphate buffer (pH 7.0) was employed as the supporting electrolyte. Electrolyte containing 10 mM of ferrocyanide/ferricyanide was utilized in the redox process of EIS. The alternating current frequencies used for impedance experiments ranged from 10 kHz to 0.1 Hz, and the amplitude  $V_{p-p}$  was  $\pm 10$  mV. The complex  $Z^*(\omega)$  (impedance) function was converted into  $C^*(\omega)$  (capacitance) through the physical definition  $Z^*(\omega) = 1/j\omega C^*(\omega)$  in which  $\omega$  is the angular frequency. All obtained impedance data were verified against the constraints of linear systems theory by using the appropriate routine of the FRA Autolab software.

### 2.3. Surfactant Adsorption on the SPCEs

Stock solutions of 0.1% Tween-20, Triton-X100, SDS, and TPAB were obtained by dissolving the required quantity in double-distilled water. Then, 5  $\mu$ L of the aforementioned surfactant solution was dripped onto SPCEs for 0–15 min to prepare various surfactant-adsorbed electrodes. Subsequently, these SPCE electrodes with adsorbed surfactants were rinsed with de-ionized water to remove excess reagents, naturally dried, and stored for later use.

### 2.4. Surfactant Adsorption on the Au Determined by QCM

Five  $\mu$ L of the surfactant solution was dripped onto Au/QCM 0–25 min to monitor various surfactant-adsorbed electrodes. For QCM measurement, the frequency shift was recorded by a time-resolved EQCM system (CHI401, CH Instruments, Inc., Austin, TX, USA) at the QCM initial resonant frequency (8 MHz) with 0.1 s of sample interval.

## 3. Results

### 3.1. Simulation and Equivalent Circuits Verification of ECS

Detailed information regarding the simulation can be obtained from the Section S.1 of Supplementary Material. The Nyquist impedance plot is characterized by a semi-circular locus that converges at the origin and at  $R_{ct}$  in high- and low-frequency ranges, respectively,

and is commonly used in EIS to simulate an electrode–electrolyte interface (as shown in Figure 1a,b) [39]. The frequency at the maximum of the imaginary part and the time constant of dielectric relaxation are affected by the complex capacitance ( $C_{dl}$  or  $C_m$ ). In ECS Nyquist plots, complex capacitances exhibit vertical lines and converged points on the real axis for all time constants, and the intercept points of the real axis in the complex impedance and capacitance intuitively present  $R_{ct}$  (or  $R_m$ ) and  $C_{dl}$  (or  $C_m$ ), respectively (Figure S1). These advantages of using ECS Nyquist plots for distinguishing various capacitances parallel to a fixed resistance in electrochemical impedance measurements are demonstrated by the simulation results.

In the verification study, electronic dummy cells were used to model electrochemical systems and verify their effectiveness through electrochemistry experiments. The effectiveness was verified by observing similar semi-circle patterns in Nyquist impedance plots (Figure 2) obtained from experimental EIS compared to simulations (Figure S1), with complete semi-circles observed for short time constants and partial semi-circles for larger time constants. A detailed discussion is provided in the supplementary material. The complex capacitance calculated from Nyquist plots was consistent with simulation results and nominal capacitor values. Further model verification was performed using electronic dummies with constant  $C_{dl}/C_m$  in parallel with varying  $R_{ct}$ , which showed consistent results in ECS Nyquist capacitance plots.

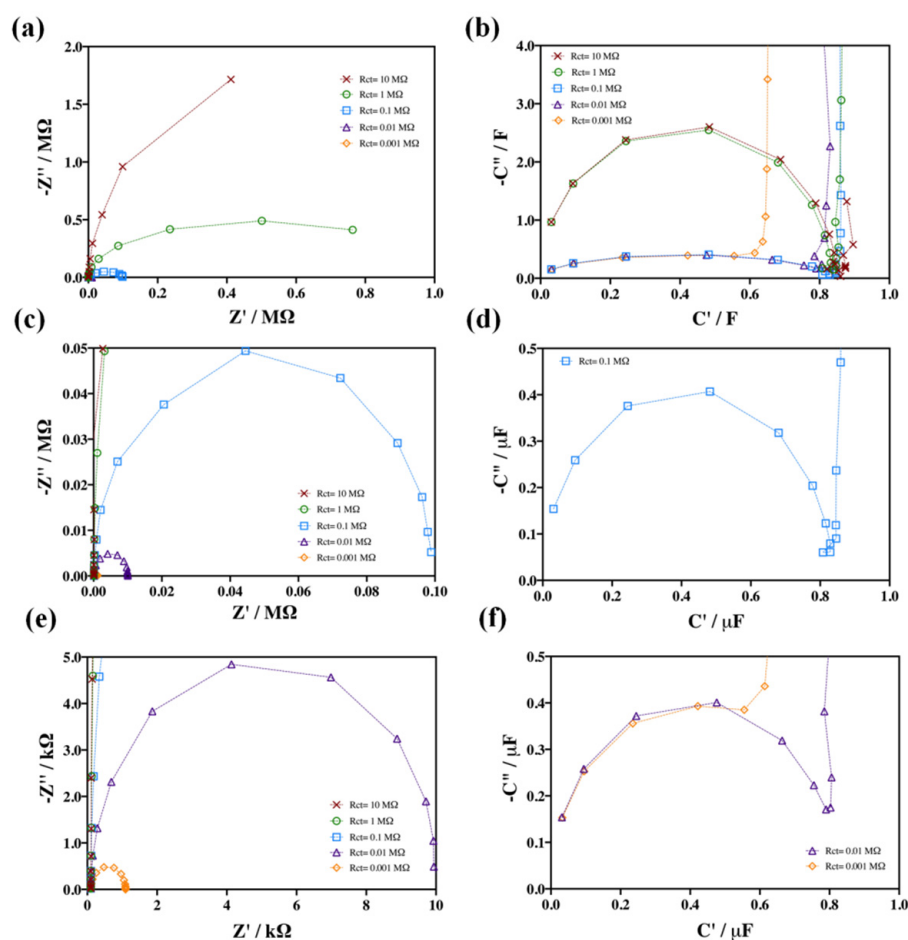


**Figure 2.** EIS and ECS validation of dummy cells with various  $R_{ct}$ . (a) EIS of an electronic dummy cell consisting of  $R_s$ ,  $C_{dl}$ , and  $R_{ct}$ , as shown in Figure 1a. (b) ECS calculated from (a). (c,e) are zoom-in plots of (a); (d,f) are zoom-in plots of (b).  $R_s = 100 \Omega$ ;  $C_{dl} = 1.0 \times 10^{-6} \text{ F}$ ;  $\times$ :  $R_{ct} = 10 \text{ M}\Omega$ ;  $\circ$ :  $R_{ct} = 1 \text{ M}\Omega$ ;  $\square$ :  $R_{ct} = 0.1 \text{ M}\Omega$ ;  $\triangle$ :  $R_{ct} = 0.01 \text{ M}\Omega$ ;  $\diamond$ :  $R_{ct} = 0.001 \text{ M}\Omega$ . The frequency range is 0.2 Hz–10 kHz.

The integrity and imaginary value of the semi-circle patterns of Nyquist plot loci in EIS and ECS, respectively, are affected by a high interfacial resistance ( $R_{ct}$  or  $R_m = 1$  or  $10\text{ M}\Omega$ ). In the ECS plots (Figure 2b,d,f), the shapes of the integrity of the semi-circle loci were not negatively affected by smaller resistances ( $R_{ct} \leq 0.1\text{ M}\Omega$ ) but only by the magnitude of imaginary capacitance values ( $C''$ ), which are noncritical for quantitative analysis. These results indicate that EIS is a useful and intuitive approach for determining lower interfacial resistance but useless for investigating higher interfacial resistance ( $R_{ct} \geq 1\text{ M}\Omega$ ). Furthermore, it is indicated that ECS is a useful and intuitive approach for determining  $C_{dl}$  or  $C_m$  under all conditions despite a high-resistance interface. The present results indicate that ECS can be complementary to EIS in investigating interfaces with highly resistive interfaces and imply that a redox couple is not necessarily required to explore solid–liquid interfaces because the interfacial capacitance is an effective and sufficient parameter. This implicit potential is fully explored in the following subsections.

### 3.2. Redox and Redoxless EIS/ECS on Bare SPCE

The capability of ECS without any redox couple (redoxless ECS) in the electrolyte was assessed using a bare SPCE and an SDS-adsorbed SPCE (SDS/SPCE) as typical conductive and resistive-permissive electrode interfaces. The integrity of the semi-circle locus and its intercept of the real axis were used as qualitative and quantitative indices in EIS as well as ECS Nyquist plots.

For the SPCE, atypical locus patterns were observed in redoxless EIS, whereas typical semi-circle loci were obtained in EIS with a redox couple (redox EIS) (Figure 3a,b). An  $R_{ct}$  value of  $38\text{ k}\Omega$  was straightforwardly obtained from the redox EIS Nyquist plots (Figure 3b), but could not be determined through redoxless EIS (Figure 3a). Both redox ECS (Figure 3d) and redoxless ECS (Figure 3c) were found to generate semi-circle loci and an approximate  $C_{dl}$  value of  $0.1\text{ }\mu\text{F}$ . The consistency of the  $C_{dl}$  values obtained from redox versus redoxless ECS demonstrated that the complex capacitance was independent of the use of redox couples in the electrolyte. In redox ECS (Figure 3d), the imaginary value at the lowest imaginary point was larger than that in redoxless ECS (Figure 3c), which can be attributed to the diffusion effect of the redox couple in EIS (Figure 3b). Atypical locus patterns of ECS with lines slightly deviating from the vertical axis were found in a lower frequency range for both redox ECS and redoxless ECS. Despite the ECS response loci of redoxless ECS being slightly different from the theoretical model simulation (Figure S1b) and experimental results obtained using electronic dummies (Figure 2b), redoxless ECS showed favorable repeatability. The typical semi-circle locus patterns in both types of ECS should be effective information for characterizing the permittivity–capacitance of an electrode interface. Compared with redox ECS, redoxless ECS of the SPCE was found to result in better patterns of typical semi-circle loci for the intuitive determination of  $C_{dl}$  in the Nyquist capacitance plots.  $C_{dl}$  for the electrode interface from ECS could be intuitively determined from the intercept of the real axis or calculated from the semi-circle fitting curve.

In summary, for lowly resistive electrode surfaces, redox EIS performed through the Faradaic process to determine  $R_{ct}$  and redoxless ECS performed through the non-Faradaic process to obtain  $C_{dl}$  is the optimal analysis strategy. This also implies complementarities of the two approaches in the assessment of an electrode interface. The usability of these two methods for assessing highly modified interfaces will be detailed in a subsequent part.

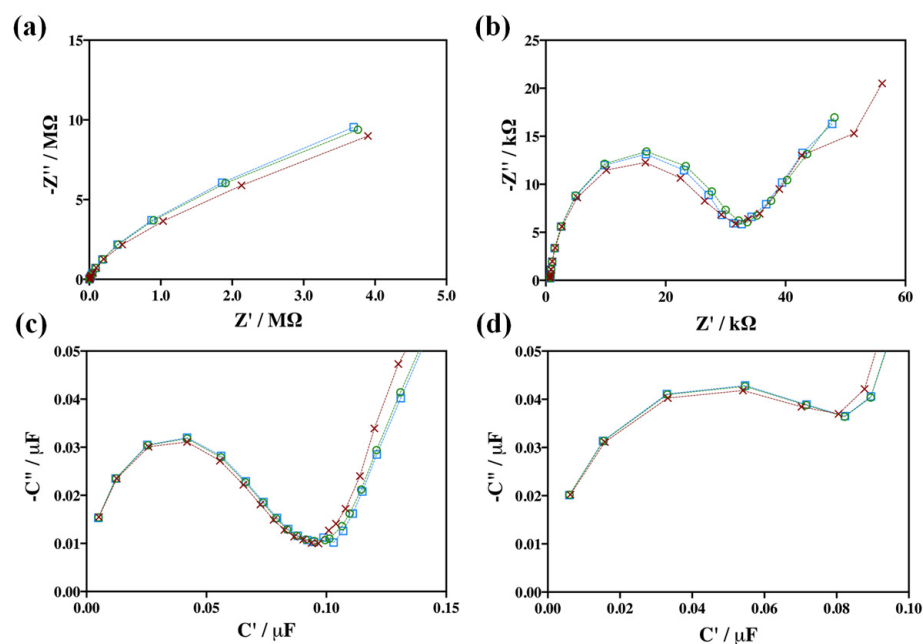


**Figure 3.** Redoxless and redox EIS as well as ECS of bare SPCEs. (a) Redoxless EIS Nyquist plots of SPCEs (area = 0.45 mm<sup>2</sup>). (b) Redox EIS Nyquist plots of SPCEs. (c) Redoxless ECS Nyquist plots calculated from (a). (d) Redox ECS Nyquist plots calculated from (b). Redoxless EIS was performed at the bias +0.0 V vs. Ag/AgCl in 0.1 M phosphate buffer (pH 7.0); redox EIS was conducted at the bias +0.3 V in the presence of 10 mM [Fe(CN)<sub>6</sub>]<sup>3−/4−</sup> in 0.1 M phosphate buffer (pH 7.0). The AC frequencies for EIS experiments ranged from 10 kHz to 0.1 Hz with an amplitude  $V_{p-p}$  of  $\pm 10$  mV.  $N = 3$ .

### 3.3. Redox and Redoxless EIS/ECS for SDS Adsorbed on SPCE

Figures 3 and S2 depict the Nyquist locus of EIS/ECS measurements for bare and SDS-adsorbed SPCEs, respectively. The reproducibility of these studies on different batches of SPE is excellent, as evidenced by consistent Nyquist locus profiles for redoxless ECSs on both bare SPCEs (Figure 3c) and SDS-adsorbed SPCEs (Figure S2c). Furthermore, the deviations in capacitances calculated from the semi-circular locus of redoxless ECSs are below 3% in both conditions. Compared to redox EIS and ECS, redoxless ECS demonstrates significantly superior reproducibility and more pronounced semi-circular locus characteristics, regardless of whether it is performed on bare or SDS-adsorbed electrodes. These results suggest that redoxless ECS offers the best capability for quantitatively analyzing the adsorption of small molecules on the interface.

The Nyquist plots were found to exhibit atypical semicircle loci for redox EIS (Figure 4b) and redox ECS (Figure 4d) in the case of SDS/SPCE. The atypical locus was attributed to the presence of a highly resistive and/or dielectric adsorption layer of SDS on the electrode surface, which resulted in limited information that could not be effectively used for model fitting and determining parameters such as  $R_{ct}$  or  $C_{dl}$ . Similarly, the redox EIS (Figure 4b) pattern showed atypical loci indicative of a highly resistive interface ( $R_{ct}$  or  $R_m = 10$  MΩ) as shown in Figure 3a, making it unsuitable for determining interfacial resistance or capacitance. Additionally, the redox ECS (Figure 4d) pattern displayed slightly-larger-than-quarter-circle loci, similar to the patterns shown in Figure 3d. Notably, the redoxless ECS Nyquist plots (Figure 4c) exhibited major and typical semi-circle loci for SDS/SPCE, demonstrating favorable repeatability, with a determined modified layer capacitance  $C_m$  of 3.8 μF. This capacitance value for SDS/SPCE differed significantly from the double-layer capacitance  $C_{dl} = 0.1$  μF of the SPCE (Figure 3c,d). Unfortunately, the redox EIS was found to be inadequate in characterizing the electrode interface with a highly resistive modified layer, whereas redox ECS proved to be more competent in this regard. Compared to redox ECS, the redoxless ECS capacitance plot showed an excellent integrity of the semi-circle locus, with its intercept on the real axis serving as qualitative

and quantitative indices, respectively. These results demonstrate that redoxless ECS can be exceptionally used to characterize the interface of a modified electrode, even in the presence of a considerably resistive modified layer.

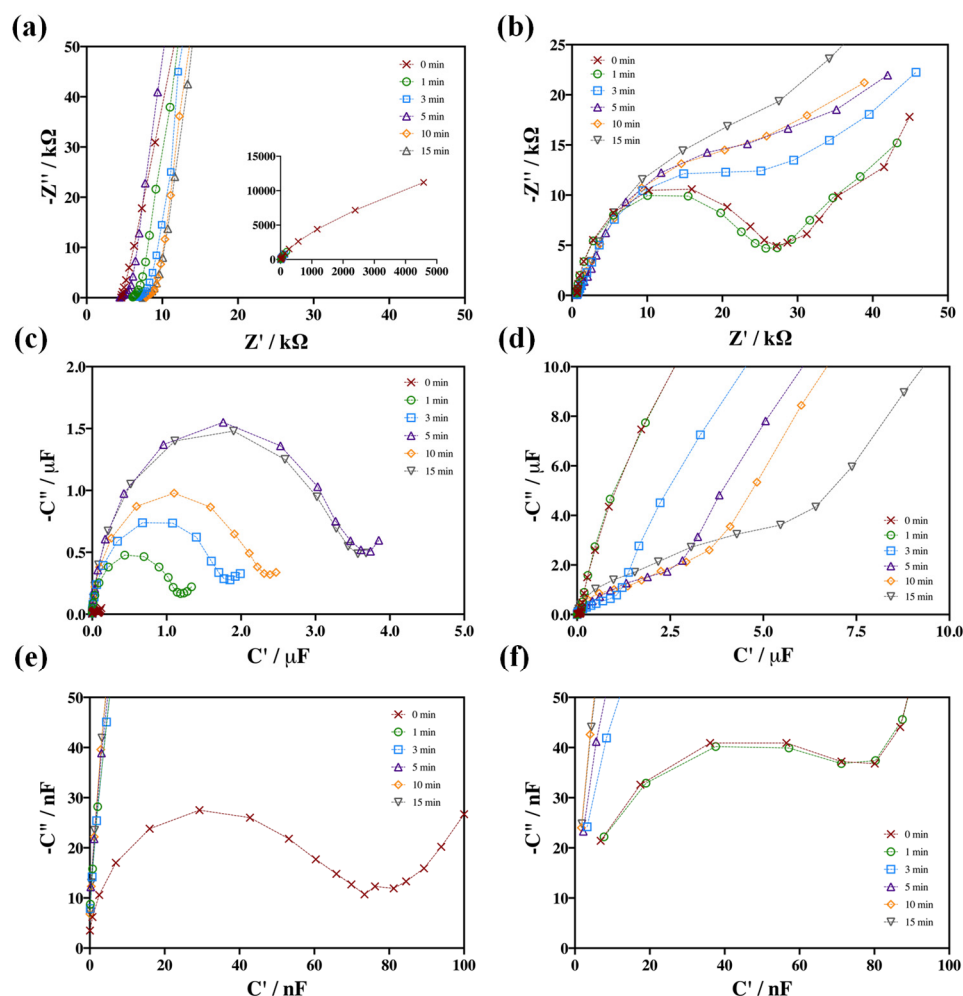


**Figure 4.** EIS and ECS Nyquist plots for SDS/SPCEs under various incubation times of SDS adsorption. Effect of incubation time for SDS adsorption onto the SPCE: (a) redoxless EIS Nyquist plots (area = 0.45 mm<sup>2</sup>); (b) redox EIS Nyquist plots; (c) redoxless ECS Nyquist plots calculated from (a); (d) redox ECS Nyquist plots calculated from (b). (e,f) are zoom-in plots of (c,d), respectively. SDS/SPCE was prepared using 5  $\mu$ L of 0.1% SDS dripped on an SPCE for 0–15 min. The symbols indicating absorption time are displayed as follows: 0 min (X), 1 min (O), 3 min (□), 5 min (△), 10 min (◇), and 15 min (▽). Experimental conditions of electrochemistry are same as for Figure 2.

The high capability to discriminate interfacial capacitances in both a bare electrode (SPCE) and highly adsorbed electrode (SDS/SPCE) was exhibited by the redoxless ECS approach. Conventional redox EIS is a well-known technique that requires a redox couple for the interfacial characterization of metals and development of biosensors. The electron mediators (probes) between the electrode and solution, which strongly reduce  $R_{ct}$  to less than 1 k $\Omega$ , are provided by the added redox pair free in the electrolyte, resulting in a typical semi-circle locus in EIS Nyquist plots. These biosensors based on EIS rely on changes in  $R_{ct}$  resulting from a modified layer and molecular recognition. Therefore, the use of redox couples is necessary and cannot be omitted in these conventional approaches. The construction of functional modifiers on electrodes, which present a typical semicircle locus in Nyquist plots for the effective determination of  $R_{ct}$  through curve fitting, has been the focus of the vast majority of research. ECS with a redox-tethered modification, also called the reagentless approach, was proposed so that a redox couple would not need to be added

to the electrolyte [16]. However, a bias potential equal to the formal potential of the redox couple is still required for EIS and/or ECS to be performed in redox-tethered ECS. Insight into interfacial characterization by using redoxless ECS was implied in a previous report of the dielectric model of modified non-electroactive interfaces through ECS [40].

Our finding indicates that a potent redoxless ECS for exploring interfacial characteristics and a realizable vision in the development of a label-free and redoxless (reagentless) biosensor based on ECS are provided by our approach. In the next subsection, surfactant adsorption on the SPCE is employed as a model for assessing the suitability of ECS for quantifying the interfacial capacitance of electrodes.

### 3.4. ECS Nyquist and Bode Plots Analysis for Adsorption of SDS on SPCE

The dependence of impedance and capacitance on incubation time for adsorption, obtained through redox or redoxless EIS or ECS, is shown in Figure 4. Fairly limited information was obtained from redoxless EIS (Figure 3a) because the interfacial impedance is extremely large and cannot present a typical EIS semicircular locus. Additionally, in the protocol involving a redox couple free in the electrolyte, both redox EIS (Figure 4b) and redox ECS (Figure 4d,f) provided less information for SDS adsorption on SPCE. Notably, favorable discrimination to time in SDS adsorption on the SPCE was exhibited by redoxless ECS (Figure 4c,e).

In both redox EIS and ECS (Figure 4b,c,f), typical semi-circle loci of Nyquist impedance and capacitance plots were discovered only for short incubation times (0 and 1 min); atypical patterns that could not be used to determine  $C_{dl}$  or  $C_m$  were obtained for incubation times longer than 3 min when highly resistive interfaces were formed. In redoxless ECS, all Nyquist capacitance plots contained typical semi-circle loci for the intuitive determination of  $C_{dl}$  or  $C_m$ , and the capacitance increases were dependent on the incubation time (varied from 0 to 15 min). The values of  $C_{dl}$  and  $C_m$  were determined to be 80 nF and 4.0  $\mu$ F, respectively, for the bare SPCE (0 min) and SPCE with a complete adsorption of SDS ( $\geq 10$  min). An excellent discriminative ability for various coverages (from null to complete) of SDS adsorption on the SPCE was exhibited by redoxless ECS (Figure 4c,e). Unfortunately, distinguishing between low coverage (incubation time = 1 min) and 0% coverage (incubation time = 0 min; Figure 4b,e,f) was difficult due to the influence of the Faradaic process and the dominant redox couple in EIS and ECS examinations of the electrode surface.

Notably, the low-coverage electrode surfaces could not be effectively distinguished, and the atypical semicircular loci in the Nyquist plot at high coverage could not be used for quantitative analysis in redox EIS or ECS. These two drawbacks limit the capability of these methods for quantitative or semi-quantitative investigations of non-electroactive layers at interfaces.

Redox and redoxless EIS and ECS were compared in the frequency domain using Bode impedance plots, as shown in Figures 5 and S4. Limited information for characterizing the interfacial properties of SDS/SPCE in the frequency domain was observed in both redoxless (Figure 5a) and redox (Figure 5b) Bode impedance plots, consistent with the Nyquist impedance plots (Figure 4a,b). However, rich information for characterizing SDS/SPCE was obtained from the Bode phase plots (Figure 5c,d). In the redoxless approach, typical sigmoid loci were observed in the Bode phase plots (Figure 5c) for all SDS/SPCE conditions, indicating excellent dielectric characteristics of the electrode interfaces examined using redoxless ECS. On the other hand, non-sigmoid loci of the Bode phase plots were obtained for the redox EIS approach (Figure 5d), indicating a considerable decrease in phase change due to the conductive and diffusion effects of the redox couple in the electrolyte at low frequencies ( $f < 1$  Hz), which may interfere with the SDS adsorption on the SPCE with an amplitude of 10 mV. Moreover, discrimination between the low coverage of SDS on the electrode (after 1 min) and the control coverage (after 0 min) was not possible, consistent with the Nyquist capacitance plot result (Figure 4f). The results from the Bode phase plots indicate that the redoxless approach exhibits complete typical locus characteristics of fine dielectric layers on the electrode surface, which are beneficial for the quantitative determination of

interfacial permittivity/capacitance through module fitting, constant-frequency methods at approximately  $f = 10 \text{ Hz}$ , or the constant phase-shift method at  $-45^\circ$ .

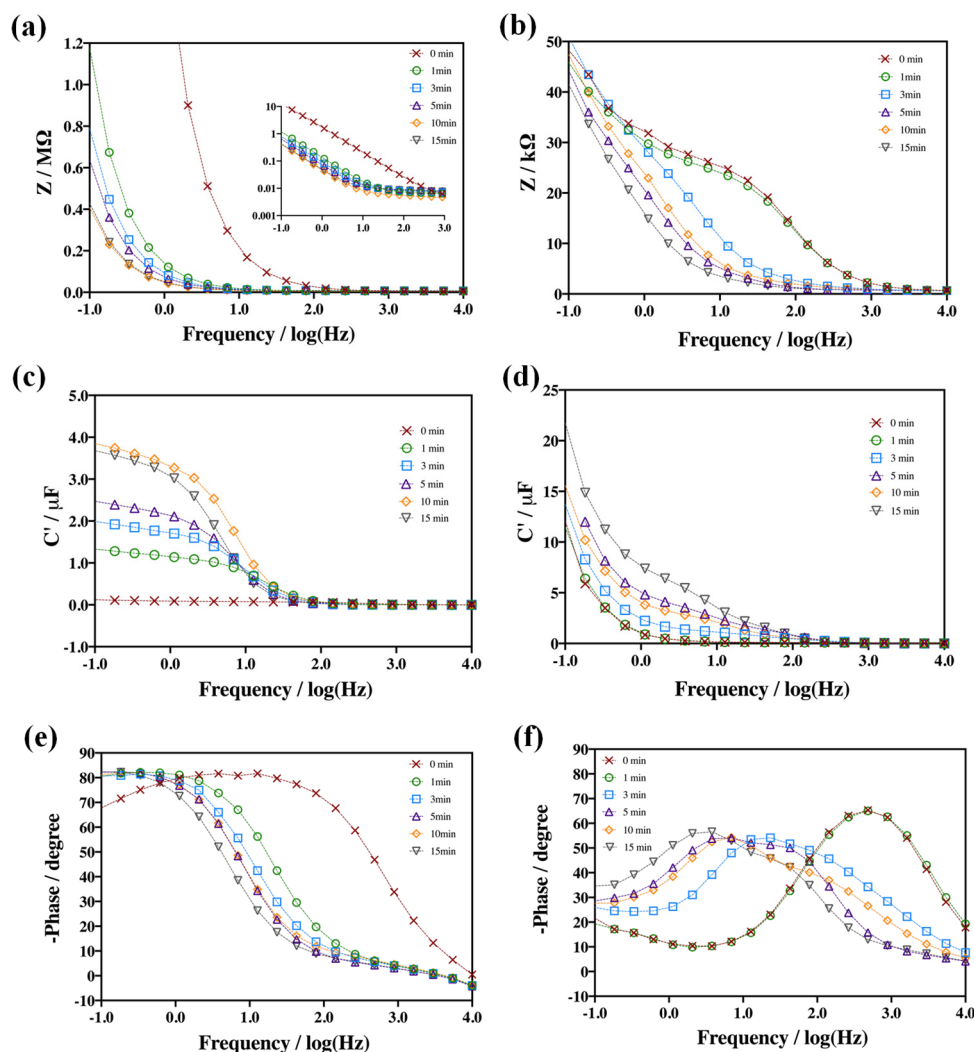


**Figure 5.** Bode plots for SDS/SPCEs under various incubation times of SDS adsorption. (a) Redoxless EIS Bode impedance plots (area =  $0.45 \text{ mm}^2$ ); (b) redox EIS Bode impedance plots; (c) redoxless ECS Bode capacitance plots; (d) redox ECS Bode capacitance plots; (e) redoxless ECS Bode phase plots; (f) redox ECS Bode phase plots. The symbols indicating absorption time are displayed as follows: 0 min ( $\times$ ), 1 min ( $\circ$ ), 3 min ( $\square$ ), 5 min ( $\triangle$ ), 10 min ( $\diamond$ ), and 15 min ( $\nabla$ ). Experimental conditions of electrochemistry are same as for Figure 3.

The interfacial impedance in both redox and redoxless EIS was dominated by resistance, as observed from the Bode resistance ( $Z'$ ) plots (Figure S3a,b), and almost identical characteristics were found in the Bode impedance ( $Z$ ) plots (Figure 5a,b). These results are consistent with the EIS Nyquist impedance plots (Figure S2a,b), revealing that a poor quantitative description of SDS adsorbed on an SPCE was offered by EIS. Despite the Bode real capacitance ( $C'$ ) plots showing a monotonic change in the real capacitance with an increase in the incubation time (Figure 5d), the limited discrimination indicated that redox EIS/ECS was unsuitable for the quantitative determination of the permittivity (capacitance) of the electrode interface. Notably, almost horizontal plateaus in a frequency range of 0.1–2 Hz with capacitance of 1.3–3.8  $\mu\text{F}$  for SDS/SPCE after various incubation times (0–15 min) were revealed by the Bode real capacitance ( $C'$ ) plots displayed in Figure S3c.

In summary, the results obtained from the Bode capacitance plots reveal that the redoxless approach had excellent typical loci characteristics of fine dielectric layers on an

electrode surface, making it beneficial for the quantitative determination of interfacial capacitance (permittivity) through constant-frequency methods in the low-frequency range (0.1–2 Hz). This characteristic offers the possibility of implementing probeless capacitive biosensors based on a single-frequency determination of capacitance in the low-frequency range.

### 3.5. Effect of Biased Potentials Applied to EIS/ECS

DC bias potential applied to electrodes affects the arrangement and characteristics of biochemical molecules on the electrode surface. The standard potential of the ferri/ferrocyanide couple on a bare glassy carbon electrode is equal to +0.265 V. Here, the dependence on adsorption may be important. In redox EIS, the DC bias should be set at the formal potential of the redox couple being employed (e.g., +0.3 V for the ferri-cyanide/ferrocyanide couple used in EIS). The bias potential used for redoxless EIS/ECS is generally set at null (+0.0 V) or the open circuit potential of the electrode to minimize energy stress on the tested electrode. Null, positive (+0.3 V), and negative (−0.3 V) DC-bias potentials were applied to SDS/SPCE in this study for investigating impedance and capacitance responses from Nyquist impedance, Nyquist capacitance, and Bode phase plots.

The redoxless EIS, redoxless ECS, and phase–frequency responses of SDS/SPCE are displayed in Figure 6. The three plots contain information from different perspectives for characterizing SDS/SPCE under various bias conditions. There were similar locus patterns in the EIS, ECS, and phase–frequency diagrams for the two conditions of null bias and positive bias ( $V = +0.3$  V), but significantly different plots were obtained for the negative bias condition ( $V = -0.3$  V). This information indicates that the SDS-adsorbed layer on the SPCE surface was considerably changed by the negative bias applied to the electrodes but negligibly altered when a positive bias of +0.3 V was applied. The former result is consistent with a previous report [41] indicating that adsorbed SDS aggregates are removed from an electrode surface under a negative potential of −0.4 V versus a saturated calomel electrode (SCE). The ionic surfactant SDS is adsorbed on the SPCE surface through a hydrophobic interaction. Electrostatic attraction may only slightly affect the SDS layer on the electrode surface, but electrostatic repulsion results in the desorption of the SDS layer.

The full-coverage SDS/SPCE had a high impedance (>40 k $\Omega$ , Figure 4b) and capacitance (3.5  $\mu$ F, Figure 6b). Its characteristics indicated a typical insulation-coated electrode with a Bode phase plot that was a sigmoid locus, as shown in Figure 6c. Under a bias of +0.3 V, the Nyquist impedance, Nyquist capacitance, and Bode phase plots were similar to those obtained under null bias (+0.0 V), but the resistance  $R_m$  and capacitance  $C_m$  were slightly higher (Figure 6a) and lower (Figure 6b), respectively. The slight changes in the SDS layer under positive DC bias did not alter the characteristic of an insulation-coated electrode (Figure 6c) but only made slight changes to the resistance and capacitance. Under a bias of −0.3 V, the resistance ( $Z'$  in Nyquist impedance plot) was considerably less than blank (+0.0 V), but the capacitance could not be precisely determined because the Nyquist capacitance plot had an atypical locus pattern (Figure 6b). The Bode phase plot (Figure 6c) under a bias of −0.3 V contained a non-sigmoid locus that exhibited a phase change to  $-40^\circ$  at the low-frequency range ( $f \leq 1$  Hz). The negatively biased SDS/SPCE could be characterized as a polymer-coated electrode partially degraded by the formation of pores [11].

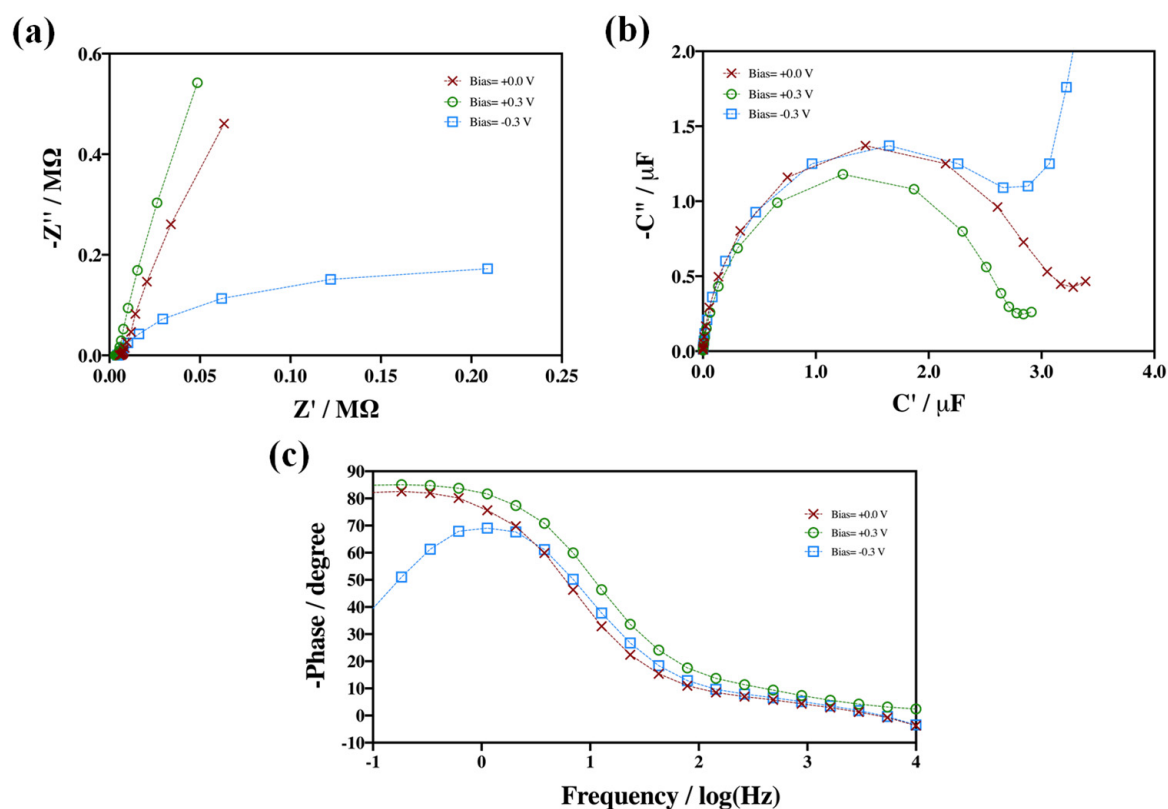


**Figure 6.** Relationship between impedance/capacitance changes and the control potential for SDS/SPCE under three potential control modes. EIS bias potential was set as +0.0 V (X), +0.3 V (O), or −0.3 V (□). (a) Redoxless EIS Nyquist impedance plots; (b) redoxless ECS Nyquist capacitance plots; (c) redoxless EIS Nyquist Bode phase plots. Experimental conditions of electrochemistry are same as for Figure 2.

Both redox and redoxless ECSs of SDS/SPCE were also performed at a bias of +0.3 V to assess the suitability of ECS Nyquist capacitance plots for the determination of real capacitances  $C'$  (Figure 7). In the ECS analysis of modified electrodes with a high resistance/impedance, the redox couples used in the electrolyte did not improve the typical Nyquist capacitance plots. Notably, redoxless ECS resulted in the semi-circular locus of a typical Nyquist plot with a negligible relationship to the interfacial impedance. This capability will be beneficial for the quantitative analysis of high-resistance/impedance modified layers, such as SAMs or non-conductive polymers, through their capacitive response. Dodecyl sulfate anions effectively adsorbed on the surface of the SPCE, forming an insulating layer (high resistance/impedance) on the surface, in a 0.1% SDS solution. SDS/SPCE also performed as an insulation-coated electrode and had a very slightly altered impedance and capacitance when a positive DC bias of +0.3 V was applied to the electrode. When the applied bias was negative ( $V = -0.3$  V), the adsorption layer acted like a porous polymer coating.

The redoxless ECS approach could be used to investigate characteristics of modified layers on an electrode surface under bias control. Moreover, null-bias redoxless ECS provided a natural microenvironment without electrostatic and electromotive forces in developing biosensors with no stress on the biomolecules immobilized on the electrode surface. The unstressed condition in null-bias redoxless ECS addresses a doubt regarding the molecular charge in affinity biosensors when performing EIS with a redox couple [15].

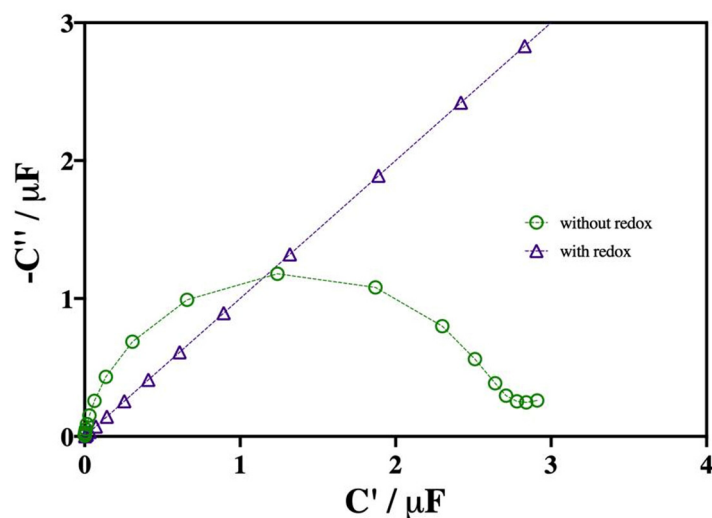


**Figure 7.** Redox couple effects in ECS of SDS/SPCE as applied with bias of +0.3 V.  $\Delta$ : With redox;  $\circ$ : without redox. Redoxless EISs were conducted at the bias +0.3 V vs. Ag/AgCl in the presence of 10 mM  $[\text{Fe}(\text{CN})_6]^{3-/4-}$  in phosphate buffer. The AC frequencies for EIS experiments ranged from 10 kHz to 0.1 Hz with an amplitude of 10 mV.

### 3.6. Surfactant Adsorption on an SPCE Investigated through Redoxless ECS

Small-molecule surfactants with different charges and shapes were used to characterize the interfacial interactions in biosensors, making them a suitable model. In this study, the redoxless ECS sensing capability was assessed using Tween-20, Triton-X100, SDS, and TPAB, which can serve as a sensing platform for biosensor development. The first two of these adsorbents are long-chain nonionic molecules, the third is a long-chain anionic molecule, and the last is a quasi-spherically cationic molecule.

Capacitance changes caused by surfactant adsorption on the SPCE surface were determined from the intercepts of the real axis in the fitted curves of semi-circle loci of ECS Nyquist capacitance plots (such as Figure 4c). The capacitance versus incubation time, obtained from the redoxless ECS plot diagrams of surfactant/SPCE in the incubation time range of 0–15 min, is presented in Figure 8. It was observed that TPAB showed negligible adsorption but the other surfactants showed high adsorption on the SPCE. Furthermore, for SDS, Tween-20, and Triton-X100, and a long incubation time (i.e., >10 min), the capacitance reached almost saturation, remaining at approximately 3.5–4.0  $\mu\text{F}$  even for an extremely long incubation time of 15 min. In the range of short incubation times (i.e., 0–5 min), a major difference was observed between the anionic SDS and nonionic Tween-20 and Triton-X100. Some difference was noted at an incubation time of 1–5 min; the capacitance of Tween-20/SPCE was almost the same as that of Triton-X100/SPCE but significantly higher (~60%) than that observed for SDS/SPCE adsorption.

These quantitative results imply that surfactant adsorption strongly influenced interfacial capacitance for the SPCE. The nonionic and long-chain surfactants (i.e., Tween-20 and Triton-X100) exhibited extremely fast adsorption on the SPCE. However, lower adsorption kinetics were observed for the anionic and long-chain SDS, and negligible adsorption was found for the cationic and non-long-chain TPAB.

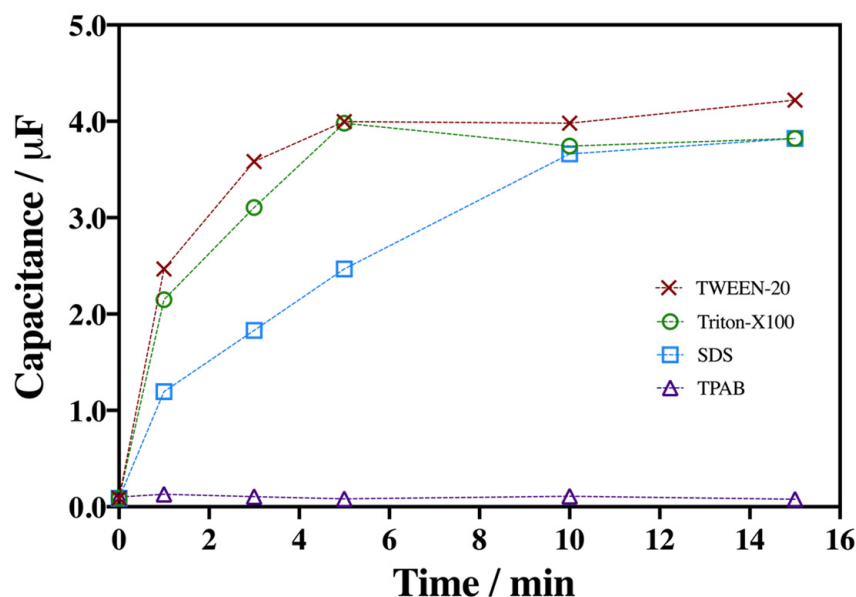


**Figure 8.** Typical calibration plots of capacitance versus incubation time for surfactant adsorption on an SCPE in 0.1 M phosphate buffer (pH 7.0), determined through redoxless ECS. Surfactants (0.1%): ×: Tween-20; ○: Triton-X100; □: SDS; △: TPAB. Experimental conditions of electrochemistry are same as for Figure 2.

### 3.7. Surfactant Adsorption on Gold Electrodes Investigated by QCM

QCM was employed in this study to gather mass information for characterizing the phenomena of surfactant adsorption at the interface. It was assumed in this work that the gold electrode on the QCM surface is also hydrophobic, similar to the carbon on the SPCE. It is hoped that the introduction of another parameter will help in understanding the adsorption phenomenon and comparing the performance of capacitance sensing.

The mass change versus incubation time obtained from the QCM response for the surfactant/Au is shown in Figure 9, indicating that TPAB shows negligible changes in frequency (mass) whereas other surfactants exhibit significant differences compared to the blank. Tween-20 tends to have a stable and significant difference from the blank in a brief period. The response time (the time required to reach a steady state) under SDS conditions takes approximately 10 min, similar to the capacitance response type in the previous Section 3.6. Triton-X100 has a significant initial value difference and tends to saturation after approximately 10 min, slightly slower than the capacitance response speed in Figure 8. The results suggest that the mass and capacitance characterizations are consistent with the adsorption behavior of TPAB and SDS surfactants, but apparent differences are observed for nonionic and long-chain surfactants (i.e., Tween-20 and Triton-X100). Most notably, the adsorption behavior of cationic and anionic surfactants exhibits distinct differences in the steady-state responses to mass and capacitance. The QCM signal at the steady state can effectively distinguish between surfactants, but the capacitance value does not exhibit such a distinction. These differences in behavior may be attributed to material properties and/or surface roughness, but further discussion on this topic is beyond the scope of this study.

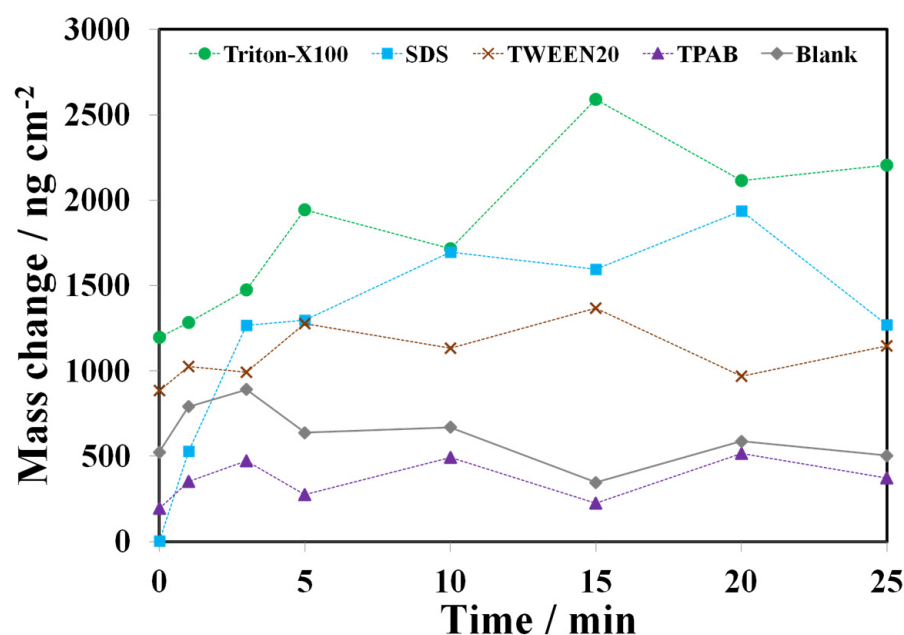


**Figure 9.** Typical mass change response of QCM versus incubation time for surfactant adsorption on gold electrode in 0.1 M phosphate buffer (pH 7.0). Surfactants (0.1%): ×: Tween-20; ●: Triton-X100; ■: SDS; ▲: TPAB; ◆: Blank (DI-water). Experimental conditions are same as for Figure 7. The sensing area of Au electrode on QCM is c.a. 0.196 cm<sup>2</sup>.

#### 4. Discussion

Surfactants adsorb in aqueous systems through hydrophobic and electrostatic interactions. Hydrophobic regions on the substrate interact with surfactant tail groups, especially on hydrophobic surfaces such as graphite [35]. TPAB has a quasi-spherical shape without a hydrophobic long chain, whereas other surfactants have linear shapes with varying alkyl chain lengths [36]. The results in Figure 7 indicate that the adsorption of surfactants on the SPCE is primarily driven by hydrophobic forces, with a slight detrimental effect from electrostatic forces during short incubation times. Under long incubation times ( $\geq 10$  min), all surfactants exhibit characteristic semi-circle (Figure 4c) and sigmoid loci (Figure 5c) on the ECS Nyquist capacitance plots and Bode phase plots, respectively, except TPAB. This suggests that the high coverage of adsorbed layers on the SPCE surface depends on the surfactant's molecular shape (long chain or semi-spherical) but is independent of its charge type. The maximum capacitances for the SPCE completely covered by the surfactant are almost identical (3.5–4.0  $\mu\text{F}$ ), indicating that the redoxless ECS approach can determine the dielectricity of the modified layer on the electrode surface. However, the QCM study does not show an identical mass response (Figure 8), which requires further investigation. This study provides valuable insights into differentiating the adsorption of nonionic and ionic surfactants on SPCEs. Redoxless ECS is a direct method for determining interfacial capacitance without the need for a redox couple or molecule immobilization on the electrode surfaces. Therefore, redoxless ECS complements label-free sensors such as QCM and surface plasmon resonance (SPR) in exploring the physicochemical characteristics of modified layers on electrodes [37,38].

New technologies are needed to understand the complex process of molecular adsorption in biomaterial and biosensor communities. It is generally believed that biochemical molecules undergo denaturation primarily through conformational changes induced by hydrophobic interaction with the material surface after initial attachment in a random orientation [42,43]. Developing novel sensing systems that provide insights into biomolecule binding and enable in situ adsorption kinetics and conformational dynamics analysis without signal contamination is crucial [44,45]. An integrated dual-function sensor with a high sensitivity for mass and permittivity changes can compare signals on a common

electrode, revealing orientation, conformational states, and affinity kinetics of adsorbed biochemical molecules [46]. Despite the potential benefits of protein surface charge heterogeneity in biorecognition and biochemical activity, the detection of proteins using intrinsic charge or a dielectric coefficient is not widely reported [47]. Previously, ion-selective electrodes had limitations in sensing depth in high-ionic-strength biological environments [48]. Larger sensing depths, such as those of QCMs, are suitable for macromolecule sensing, whereas capacitance sensors are convenient for monitoring small ionic molecules due to their inherently small sensing depth.

The classical “frequency–frequency” mode of EIS measurement, commonly used for electrochemical sensing, relies on fitting the Nyquist plot data to the Randles-type model to obtain  $R_{ct}$  as a biosensor parameter. However, time-dependent phenomena in non-stationary electrochemical sensors used for biological and chemical applications pose challenges. Scanning raw data over a wide frequency range is time-consuming and lacks the required high temporal resolution for real-time measurements, limiting EIS development in biosensors. As a solution, researchers prefer single-frequency or single-step impedance measurements [49,50] to capture fast, real-time interface phenomena. The selection of a characteristic frequency, typically based on a stable response and discrimination power on the Bode plot, is crucial for single-frequency measurement. In this study, the plateau-like sigmoid curve in the low frequency range of the Bode capacitance response (Figure 5c) was chosen as the characteristic frequency without redoxless ECS. However, achieving an ideal sigmoid profile for characteristic frequency selection is challenging in the impedance and phase characterization of non-high- $\kappa$  dielectric solid–liquid interfaces (Figure 1a,b). Even with a better dielectric layer on the electrode surface (as shown in Figure 5b,d,f), obtaining a plateau-like sigmoid curve in redox EIS measurements is challenging. For investigating bio-molecular affinity kinetics, a real-time and high sampling rate sensing approach is essential, which can be achieved with redoxless ECS by single-frequency measurement, meeting the requirements of probeless and real-time measurements.

While ECS has its advantages in determining interfacial capacitance without the need for a redox couple or molecule immobilization, it also has limitations in terms of mass sensitivity, differentiation based on charge type, depth of sense, and capturing time-dependent phenomena. These limitations highlight the need for further research and the development of novel sensing systems with an excellent temporal resolution that address these drawbacks and provide more comprehensive insights into molecular adsorption in biomaterial and biosensor applications.

## 5. Conclusions

In this study, a simple redoxless ECS approach was presented, which was derived from the non-Faradaic EIS approach for determining surfactant adsorption on disposable SPCEs. The feasibility of discriminating interfacial capacitances on electrode surfaces using the redoxless ECS was demonstrated through a simulation of equivalent circuit models and electrochemical tests of electronic dummy cells. The adsorption of surfactants with differing characteristics (charge and hydrophobic chain length) could be effectively distinguished, and the dynamic response of surfactant adsorption over 0–15 min could be quantitatively assayed using the proposed method. The methodology is characterized by its simplicity, reliance on a straightforward determination or simple fitting of response data, the utilization of a null-bias electrochemical test, and a lack of requirement for a redox couple as a probe in the electrolyte. This is the first report that supports a redoxless capacitive assay or sensor for the adsorption of low-molecular-weight surfactants. Importantly, the electrochemical impedance/capacitance analysis does not require a redox couple and bias potential, effectively eliminating doubts about interference caused by charge and potential in biosensor development and applications.

**Supplementary Materials:** The following supporting information can be downloaded at: <https://www.mdpi.com/article/10.3390/chemosensors11060343/s1>, Figure S1: Simulation and experimental validation by using dummy cells; Figure S2: Redoxless EIS and ECS of SDS/SPCE; Figure S3: Bode resistance and capacitance plots of SDS/SPCE under various incubation times for SDS adsorption; Section S1: Simulation—complex impedance and capacitance of an equivalent circuit with parallel  $R_{ct}$  and various capacitance  $C_{dl}$ ; Section S2: EIS and ECS of equivalent circuits verification by electronic dummy cells.

**Author Contributions:** Conceptualization, T.-J.C.; methodology, T.-J.C.; validation, H.-Y.H. and T.-J.C.; formal analysis, H.-Y.H.; investigation, T.-J.C. and H.-Y.H.; resources, T.-J.C. and R.L.C.C.; data curation, P.-C.T.; writing—original draft preparation, T.-J.C.; writing—review and editing, R.L.C.C.; visualization, P.-C.T.; supervision, T.-J.C.; project administration, T.-J.C. All authors have read and agreed to the published version of the manuscript.

**Funding:** This research received no external funding.

**Institutional Review Board Statement:** Not applicable.

**Informed Consent Statement:** Not applicable.

**Data Availability Statement:** Not applicable.

**Acknowledgments:** The authors would like to thank Bo-Chuan Hseih for technique supporting this research.

**Conflicts of Interest:** The authors declare no conflict of interest.

## References

1. Daniels, J.S.; Pourmanda, N. Label-Free Impedance Biosensors: Opportunities and Challenges. *Electroanalysis* **2007**, *19*, 1239–1257. [[CrossRef](#)] [[PubMed](#)]
2. Orazem, M.E.; Tribollet, B. *Electrochemical Impedance Spectroscopy*, 2nd ed.; John Wiley & Sons: Hoboken, NJ, USA, 2017; ISBN 9781119341222.
3. Castela, A.; Simões, A.; Ferreira, M.E.I.S. Evaluation of Attached and Free Polymer Films. *Prog. Org. Coat.* **2000**, *38*, 1–7. [[CrossRef](#)]
4. Sabot, A.; Krause, S. Simultaneous Quartz Crystal Microbalance Impedance and Electrochemical Impedance Measurements. Investigation into the Degradation of Thin Polymer Films. *Anal. Chem.* **2002**, *74*, 3304–3311. [[CrossRef](#)] [[PubMed](#)]
5. Guo, B.; Lin, X.; Fu, W.; Kua, J. Establishment of Electrochemical Methods to Examine the Adsorption of Flotation Surfactants onto a Mineral Surface. *J. Chem. Technol. Biotechnol.* **2020**, *95*, 1580–1589. [[CrossRef](#)]
6. Kouhi, M.; Mohebbi, A.; Mirzaei, M. Evaluation of the Corrosion Inhibition Effect of Micro/Nanocapsulated Polymeric Coatings: A Comparative Study by Use of EIS and Tafel Experiments and the Area under the Bode Plot. *Res. Chem. Intermed.* **2013**, *39*, 2049–2062. [[CrossRef](#)]
7. Feliu, S., Jr. Electrochemical Impedance Spectroscopy for the Measurement of the Corrosion Rate of Magnesium Alloys: Brief Review and Challenges. *Metals* **2020**, *10*, 775. [[CrossRef](#)]
8. Iurilli, P.; Brivio, C.; Wood, V. On the Use of Electrochemical Impedance Spectroscopy to Characterize and Model the Aging Phenomena of Lithium-Ion Batteries: A Critical Review. *J. Power Sources.* **2021**, *505*, 229860. [[CrossRef](#)]
9. Randviir, E.P.; Banks, C.E. Electrochemical Impedance Spectroscopy: An Overview of Bioanalytical Applications. *Anal. Methods.* **2013**, *5*, 1098–1115. [[CrossRef](#)]
10. Sibai, A.; Elamri, K.; Barbier, D.; Jaffrezic-Renault, N.; Souteyrand, E. Analysis of the Polymer-Antibody-Antigen Interaction in a Capacitive Immunosensor by FTIR Difference Spectroscopy. *Sens. Actuators B Chem.* **1996**, *31*, 125–130. [[CrossRef](#)]
11. Fernandez-Sanchez, C.; McNeil, C.J.; Rawson, K. Electrochemical Impedance Spectroscopy Studies of Polymer Degradation: Application to Biosensor Development. *TrAC—Trends Anal. Chem.* **2005**, *24*, 37–48. [[CrossRef](#)]
12. Bertok, T.; Lorencova, L.; Chocholova, E.; Jane, E.; Vikartovska, A.; Kasak, P.; Tkac, J. Electrochemical Impedance Spectroscopy Based Biosensors: Mechanistic Principles, Analytical Examples and Challenges towards Commercialization for Assays of Protein Cancer Biomarkers. *Chem. Electro. Chem.* **2019**, *6*, 989–1003. [[CrossRef](#)]
13. Sopoušek, J.; Věžník, J.; Houser, J.; Skládal, P.; Lacina, K. Crucial Factors Governing the Electrochemical Impedance on Protein-Modified Surfaces. *Electrochim. Acta.* **2021**, *388*, 138616. [[CrossRef](#)]
14. Rama, Y.; Yoetz-Kopelman, T.; Dror, Y.; Freeman, A.; Shacham-Diamanda, Y. Impact of Molecular Surface Charge on Biosensing by Electrochemical Impedance Spectroscopy. *Electrochim. Acta* **2016**, *200*, 161–167. [[CrossRef](#)]
15. Lacina, K.; Sopoušek, J.; Čunderlová, V.; Hlaváček, A.; Václavěk, T.; Lacinová, V. Biosensing Based on Electrochemical Impedance Spectroscopy: Influence of the Often-Ignored Molecular Charge. *Electrochem. Commun.* **2018**, *93*, 183–186. [[CrossRef](#)]
16. Bueno, P.R.; Mizzon, G.; Davis, J.J. Capacitance Spectroscopy: A Versatile Approach To Resolving the Redox Density of States and Kinetics in Redox-Active Self-Assembled Monolayers. *J. Phys. Chem. B.* **2012**, *116*, 8822–8829. [[CrossRef](#)]

17. da Silva, D.J.R.; Diniz, F.B. Electrochemical Impedance Spectroscopy Study of Concanavalin A Adsorption on Glassy Carbon Electrode: An Analysis of Capacitance Dispersion. *Electrochim. Acta.* **2014**, *119*, 99–105. [[CrossRef](#)]
18. Itagaki, M.; Suzuki, S.; Shitanda, I.; Watanabe, K. Electrochemical Impedance and Complex Capacitance to Interpret Electrochemical Capacitor. *Electrochemistry* **2007**, *75*, 649–655. [[CrossRef](#)]
19. Ribeiro, W.C.; Gonçalves, L.M.; Liébana, S.; Pividoric, M.I.; Bueno, P.R. Molecular Conductance of Double-Stranded DNA Evaluated by Electrochemical Capacitance Spectroscopy. *Nanoscale* **2016**, *8*, 8931–8938. [[CrossRef](#)]
20. Cecchetto, J.; Santos, A.; Mondini, A.; Cilli, E.M.; Bueno, P.R. Serological Point-of-Care and Label-Free Capacitive Diagnosis of Dengue Virus Infection. *Biosens. Bioelectron.* **2020**, *151*, 111972. [[CrossRef](#)]
21. Oliveira, R.M.B.; Fernandes, F.C.B.; Bueno, P.R. Pseudocapacitance Phenomena and Applications in Biosensing Devices. *Electrochim. Acta* **2019**, *306*, 175–184. [[CrossRef](#)]
22. Baradoke, A.; Hein, R.; Li, X.; Davis, J.J. Reagentless Redox Capacitive Assaying of C-Reactive Protein at a Polyaniline Interface. *Anal. Chem.* **2020**, *92*, 3508–3511. [[CrossRef](#)] [[PubMed](#)]
23. Piccoli, J.; Hein, R.; El-Sagheer, A.H.; Brown, T.; Cilli, E.M.; Bueno, P.R.; Davis, J.J. Redox Capacitive Assaying of C-Reactive Protein at a Peptide Supported Aptamer Interface. *Anal. Chem.* **2018**, *90*, 3005–3008. [[CrossRef](#)] [[PubMed](#)]
24. Lehr, J.; Fernandes, F.C.B.; Bueno, P.R.; Davis, J.J. Label-free Capacitive Diagnostics: Exploiting Local Redox Probe State Occupancy. *Anal. Chem.* **2014**, *86*, 2559–2564. [[CrossRef](#)] [[PubMed](#)]
25. Fernandes, F.C.B.; Santos, A.; Martins, D.C.; Góes, M.S.; Bueno, P.R. Comparing Label Free Electrochemical Impedimetric and Capacitive Biosensing Architectures. *Biosens. Bioelectron.* **2014**, *57*, 96–102. [[CrossRef](#)] [[PubMed](#)]
26. Cecchetto, J.; Fernandes, F.C.B.; Lopes, R.; Bueno, P.R. The Capacitive Sensing of NS1 Flavivirus Biomarker. *Biosens. Bioelectron.* **2017**, *87*, 949–956. [[CrossRef](#)] [[PubMed](#)]
27. Garrote, B.L.; Santos, A.; Bueno, P.R. Perspectives on and Precautions for the Uses of Electric Spectroscopic Methods in Label-Free Biosensing Applications. *ACS Sens.* **2019**, *4*, 2216–2227. [[CrossRef](#)]
28. Dionne, E.R.; Amara, F.B.; Badia, A. An Electrochemical Immittance Analysis of the Dielectric Properties of Self-Assembled Monolayers. *Can. J. Chem.* **2020**, *98*, 471–479. [[CrossRef](#)]
29. Guttenplan, A.P.M.; Bormans, S.; Birgani, Z.T.; Schumacher, M.; Giselsbrecht, S.; Truckenmüller, R.K.; Habibović, P.; Thoelen, R. Measurement of Biomimetic Deposition of Calcium Phosphate in Real Time Using Complex Capacitance. *Phys. Status Solidi A.* **2021**, *218*, 2000672. [[CrossRef](#)]
30. Assaifan, A.K.; Hezam, M.; Al-Gawati, M.A.; Alzahrani, K.E.; Alswielehe, A.; Arunachalam, P.; Al-Mayouf, A.; Alodhayb, A.; Albrithen, H. Label-free and simple detection of trace Pb(II) in tap water using non-faradaic impedimetric sensors. *Sens. Actuator A Phys.* **2021**, *329*, 112833. [[CrossRef](#)]
31. Bueno, P.R.; Hein, R.; Santos, A.; Davis, J.J. The Nanoscopic Principles of Capacitive Ion Sensing Interfaces. *Phys. Chem. Chem. Phys.* **2020**, *22*, 3770–3774. [[CrossRef](#)]
32. Tasić, N.; Cavalcante, L.; Deffune, E.; Góes, M.S.; Paixão, T.R.L.C.; Gonçalves, L.M. Probeless and Label-Free Impedimetric Biosensing of D-Dimer using Gold Nanoparticles Conjugated with Dihexadecylphosphate on Screen-Printed Carbon Electrodes. *Electrochim. Acta.* **2021**, *397*, 139244. [[CrossRef](#)]
33. Hudari, F.F.; Bessegato, G.G.; Fernandes, F.C.B.; Zanoni, M.V.B.; Bueno, P.R. Reagentless Detection of Low-Molecular-Weight Triamterene Using Self-Doped TiO<sub>2</sub> Nanotubes. *Anal. Chem.* **2018**, *90*, 7651–7658. [[CrossRef](#)]
34. Luo, X.; Xu, M.; Freeman, C.; James, T.; Davis, J.J. Ultrasensitive Label Free Electrical Detection of Insulin in Neat Blood Serum. *Anal. Chem.* **2013**, *85*, 4129–4134. [[CrossRef](#)]
35. Atkina, R.; Craigh, V.S.J.; Wanless, E.J.; Biggs, S. Mechanism of Cationic Surfactant Adsorption at the Solid–Aqueous Interface. *Adv. Colloid Interface Sci.* **2003**, *103*, 219–304. [[CrossRef](#)]
36. Fic, K.; Lota, G.; Frackowiak, E. Electrochemical Properties of Supercapacitors Operating in Aqueous Electrolyte with Surfactants. *Electrochim. Acta* **2010**, *55*, 7484–7488. [[CrossRef](#)]
37. Anastopoulos, A.G.; Papoutsis, A.D.; Papaderakis, A.A. Differential Capacitance and Electrochemical Impedance Study of Surfactant Adsorption on Polycrystalline Ni Electrode. *J. Solid State Electrochem.* **2015**, *19*, 2369–2377. [[CrossRef](#)]
38. Stålgren, J.; Eriksson, J.K.; Boschkovaab, K. A Comparative Study of Surfactant Adsorption on Model Surfaces Using the Quartz Crystal Microbalance and the Ellipsometer. *J. Colloid Interface Sci.* **2002**, *253*, 190–195. [[CrossRef](#)]
39. Bouvet, G.; Nguyen, D.D.; Mallarino, S.; Touzain, S. Analysis of the Non-Ideal Capacitive Behaviour for High Impedance Organic Coatings. *Prog. Org. Coat.* **2014**, *77*, 2045–2053. [[CrossRef](#)]
40. Góes, M.S.; Rahman, H.; Ryall, J.; Davis, J.J.; Bueno, P.R. A Dielectric Model of Self-Assembled Monolayer Interfaces by Capacitive Spectroscopy. *Langmuir* **2012**, *28*, 9689–9699. [[CrossRef](#)]
41. He, S.; Meng, Y.; Tian, Y. Correlation Between Adsorption/Desorption of Surfactant and Change in Friction of Stainless Steel in Aqueous Solutions Under Different Electrode Potentials. *Tribol Lett.* **2011**, *41*, 485–494. [[CrossRef](#)]
42. Höök, F.; Rodahl, M.; Kasemo, B.; Brzezinski, P. Structural Changes in Hemoglobin During Adsorption to Solid Surfaces: Effects of pH, Ionic Strength, and Ligand Binding. *Proc. Natl. Acad. Sci. USA* **1998**, *95*, 12271–12276. [[CrossRef](#)] [[PubMed](#)]
43. Roach, P.; Eglin, D.; Rohde, K.; Perry, C.C. Modern Biomaterials: A Review—Bulk Properties and Implications of Surface Modifications. *Mater. Sci. Mater. Med.* **2007**, *18*, 1263–1277. [[CrossRef](#)] [[PubMed](#)]

44. Reimhult, E.; Larsson, C.; Kasemo, B.; Höök, F. Simultaneous Surface Plasmon Resonance and Quartz Crystal Microbalance with Dissipation Monitoring Measurements of Biomolecular Adsorption Events Involving Structural Transformations and Variations in Coupled Water. *Anal. Chem.* **2004**, *76*, 7211–7220. [[CrossRef](#)] [[PubMed](#)]
45. Roach, P.; Farrar, D.; Perry, C.C. Interpretation of Protein Adsorption: Surface-Induced Conformational Changes. *J. Am. Chem. Soc.* **2005**, *127*, 8168–8173. [[CrossRef](#)]
46. Goda, T.; Maeda, Y.; Miyahara, Y. Simultaneous Monitoring of Protein Adsorption Kinetics Using a Quartz Crystal Microbalance and Field-Effect Transistor Integrated Device. *Anal. Chem.* **2012**, *84*, 7308–7314. [[CrossRef](#)]
47. Honig, B.; Nicholls, A. Classical Electrostatics in Biology and Chemistry. *Science* **1995**, *268*, 1144–1149. [[CrossRef](#)]
48. Poghossian, A.; Cherstvy, A.; Ingebrandt, S.; Offenhausser, A.; Schoning, M.J. Possibilities and Limitations of Label-Free Detection of DNA Hybridization with Field-Effect-Based Devices. *Sens. Actuators B Chem.* **2005**, *111*, 470–480. [[CrossRef](#)]
49. Kirchhain, A.; Bonini, A.; Vivaldi, F.; Poma, N.; Di Francesco, F. Latest developments in non-faradic impedimetric biosensors: Towards clinical applications, TrAC. *Trends Anal. Chem.* **2020**, *133*, 116070. [[CrossRef](#)]
50. Assaifan, A.K.; Alqahtani, F.A.; Alnamlah, S.; Almutairi, R.; Alkhamash, H.I. Detection and Real-Time Monitoring of LDL-Cholesterol by Redox-Free Impedimetric Biosensors. *BioChip* **2022**, *16*, 197–206. [[CrossRef](#)]

**Disclaimer/Publisher’s Note:** The statements, opinions and data contained in all publications are solely those of the individual author(s) and contributor(s) and not of MDPI and/or the editor(s). MDPI and/or the editor(s) disclaim responsibility for any injury to people or property resulting from any ideas, methods, instructions or products referred to in the content.